High-resolution EELS study of the vacancy-doped metal/insulator system, $Nd_{1-x}TiO_3$, $x = 0$ to 0.33.

Athena S. Sefat[a,b,*], Gisele Amow[c], Meng-Yue Wu[d],
Gianluigi A. Botton[a,d,e], J.E. Greedan[a,b]

[a]*Brockhouse Institute for Materials Research, McMaster University, Hamilton, Canada*
[b]*Department of Chemistry, McMaster University, 1280 Main Street West (ABB-433), Hamilton, Ont., Canada L8S 4M1*
[c]*ICPET, NRC, Montreal Road, Ottawa, Canada*
[d]*Department of Technical Science, National Centre for HREM, Delft University of Technology, Delft, The Netherlands*
[e]*Department of Materials Science and Engineering, McMaster University, Hamilton, CANADA*

Abstract

High-resolution electron energy loss spectroscopy (EELS) spectra have been obtained for several members of the vacancy-doped metal/insulator perovskite system $Nd_{1-x}TiO_3$ where $NdTiO_3$ ($x = 0$) is a Mott–Hubbard insulator and $Nd_{2/3}TiO_3$ ($x = 0.33$), a band insulator. The insulator to correlated-metal transitions occur at $x \approx 0.20$ and $x \approx 0.10$. Both O K- and Ti $L_{2,3}$-edge data were obtained on the title materials and the related d^0 perovskites, $CaTiO_3$, $SrTiO_3$ and $BaTiO_3$. The crystal structure of $Nd_{0.70}TiO_3$ ($x = 0.30$) was refined from powder neutron data in *Cmmm* which is taken as a model for the structure of $Nd_{2/3}TiO_3$ ($x = 0.33$) as well. The L-edge spectra for $Nd_{1-x}TiO_3$ show systematic changes consistent with the valence state evolution from all Ti^{3+} ($x = 0.0$) to all Ti^{4+} ($x = 0.33$). Octahedral crystal fields of 1.5 and 2.0 eV were inferred from the L-edge data for $NdTiO_3$ and $Nd_{2/3}TiO_3$ by comparison with calculated spectra from the literature. Broader L_3 and L_2 peak widths for $Nd_{2/3}TiO_3$ than for the other d^0 perovskites are attributed to the more complex crystal structure of this material which includes two Nd sites with partial occupation and a more distorted Ti–O environment with low site symmetry. A markedly different O K-edge spectrum for $Nd_{2/3}TiO_3$ is attributed to the involvement of Nd $5d$ levels.

Keywords: ELNES; Transition metal oxide; Perovskite; Titanium L-edge; Oxygen K-edge

1. Introduction

In recent years extensive, systematic studies of the electronic structure of transition metal oxides have been carried out using core-level techniques such as X-ray absorption spectroscopy (XAS) and electron energy loss spectroscopy (EELS) [1,2]. It has been shown that features of these spectra such as peak positions, fine

structures of oxygen K-edge spectra and the intensity ratio between metal L_2- and L_3-edges, $I(L_3)/I(L_2)$, are sensitive to the oxidation state of the metal ions, levels of metal ligand covalency and crystal field splittings for example [3]. The electronic structure of transition metal compounds predominately depends on their open d-shells, which contribute to the chemical bonding and are affected strongly by the surrounding ligands. EELS and XAS are complementary methods on energy and spatial resolution. In general, XAS can be carried out at higher energy resolution while EELS shows better spatial resolution in that information can be obtained even from samples of submicron dimensions. Recently, EELS

*Corresponding author. Department of Chemistry, McMaster University, 1280 Main Street West (ABB-433), Hamilton, Ont., Canada L8S 4M1. Fax: +1 905 521 2773.

E-mail address: safasea@mcmaster.ca (A.S. Sefat).

instruments using monochromated electron beams have been developed which show energy resolution rivaling that of XAS [4]. In the following work, the energy-loss *near-edge* structure (ELNES) technique is used to study the electronic structure of the mixed valence system $Nd_{1-x}TiO_3$ as the composition is changed through metal-to-insulating transitions.

The $Nd_{1-x}TiO_3$ system is a solid solution existing between two insulators: the Mott–Hubbard insulator $NdTiO_3$, and the charge-transfer-insulator $Nd_{2/3}TiO_3$ [5]. For $NdTiO_3$, the Ti^{3+} cations have the electronic configuration $3d^1$ which occupies a state of t_{2g} symmetry due to the octahedral crystal field. In the crystal strong electron correlations localize the d electrons which are said to reside in the lower Hubbard band (LHB). The LHB has finite width due to covalent interactions with the O $2p$ states. The creation of Nd^{3+} vacancies introduces holes in the LHB at the rate of 3 holes per vacancy. For $Nd_{2/3}TiO_3$ with Ti^{4+} ($3d^0$), as the lowest energy excitation removes an electron from the $2p$ to the empty d-band, this is a band insulator. Addition of Nd^{3+} ions adds electrons to the t_{2g} states. By adding electrons to the d-band of $Nd_{2/3}TiO_3$, or adding holes to $NdTiO_3$, insulating-to-metallic transitions occur at vacancy compositions of $x \approx 0.20$ and 0.10, respectively [5]. This system thus exhibits phenomena similar to those seen for related solid solutions such as $La_{1-x}Sr_x TiO_3$ [6] or $La_{1-x}TiO_3$ [7] but with significantly higher levels of electron correlation. The crystal structure of stoichiometric $NdTiO_3$ ($x = 0$) is described in *Pmna* and is isostructural to $LaTiO_3$ [8]. The same structure seems to persist for doping levels as large as $x = 0.20$. For $x > 0.20$ the structure is not known in detail but seems to be related to that found for $La_{2/3}TiO_3$ [7]. Prior to this study, $Nd_{2/3}TiO_3$ ($x = 0.33$) had not been prepared as a pure phase. Herein we report the growth of crystals of $x = 0.33$ by the flux growth method using a CsF/$Na_2B_4O_7$ flux. As well, a model for the crystal structure for $x = 0.30$ and 0.33 is proposed from power neutron data. In the following we present the ELNES K-edge and L_{23}-edge spectra for samples with $x = 0, 0.05, 0.12, 0.21$, and 0.33. The results are discussed in relation to changes in the density of unoccupied electronic states around the oxygen and titanium ions. In addition, the single valent, Ti^{4+} $Nd_{2/3}TiO_3$ spectrum is compared with those of similar perovskite compounds $BaTiO_3$, $SrTiO_3$, and $CaTiO_3$.

2. Experimental details

2.1. Sample preparation

$Nd_{1-x}TiO_3$. Polycrystalline samples of $x = 0, 0.05, 0.12, 0.21$, and 0.30 were prepared by mixing, grinding and pelletizing stoichiometric amounts of Ti_2O_3 (99.9%), pre-dried Nd_2O_3 and TiO_2 (99.9%). Each sample was sealed in a molybdenum crucible under purified argon gas. The preparation conditions involved several firing and regrinding steps at $\sim 1400\,^\circ C$ for $\sim 12\,h$. Phase purity was monitored by X-ray powder diffraction using a Guinier–Hägg camera with monochromated $CuK\alpha_1$ radiation and Si as an internal standard. The products were black in color.

$Nd_{2/3}TiO_3$. Growth of crystals of $Nd_{2/3}TiO_3$ were obtained by the flux method, in which a cesium fluoride/sodium tetraborate flux was used. The pre-dried Nd_2O_3 (0.7872 g, 99.99% Rhone Poulenc), TiO_2 (1.1161 g, 99.999% CERAC) and CsF (15.039 g, 99.999% CERAC) and $Na_2B_4O_7$ (0.993 g, 99.99% Fisher Scientific) were ground together in an inert atmosphere. The reagents were placed and sealed in a platinum crucible. The growth conditions involved heating the crucible to $1100\,^\circ C$, holding it at this temperature for $2\,h$, and then cooling to $1000\,^\circ C$ at a rate of $1\,^\circ C/h$. The crucible was then quenched at $1000\,^\circ C$ to room temperature and hot poured in order to isolate the crystals from flux. The crystals were transparent, violet plates with dimensions $\sim 1 \times 1 \times 0.25\,mm$.

2.2. Powder neutron diffraction

$Nd_{0.70}TiO_3$. Neutron diffraction data were collected for a polycrystalline sample of $Nd_{0.70}TiO_3$ using neutrons with $\lambda = 1.3920\,\text{Å}$ at the McMaster Nuclear Reactor. The sample was contained in a thin walled vanadium can at room temperature. The diffractometer has been described elsewhere [9].

2.3. EELS measurements

The near-edge electron energy loss absorption experiments reported here were performed at the Laboratory of Materials Science, Centre of HREM, Delft University of Technology, The Netherlands. The instrument used was a $200\,kV$ TEM-STEM (FEI Tecnai 200 FEG) equipped with a monochromator and a high-resolution energy loss spectrometer (a Gatan Imaging Filter model for HREELS) yielding a combined energy resolution of ~ 0.10–$0.20\,eV$ (measured at the FWHM at the zero loss peak). Details of this system and first applications in materials science (including for the measurement of bandgaps) have been described elsewhere [4]. The spectra were acquired in diffraction mode using a large ($>10\,mrad$) spectrometer collection angle and a dispersion of $0.05\,eV/channel$. For each individual sample, a number of spectra acquired for short acquisition times (between 5 and 30 s each) were added together yielding a total acquisition time varying between 30 and 300 s. The TEM samples for EELS measurements were prepared by crushing the solid solution powder in ethanol and by dispersing the suspension on a holey carbon-covered Cu

grid. For each sample, several particles were analyzed. The reference materials ($BaTiO_3$, $SrTiO_3$, $CaTiO_3$) were prepared in a similar way although the total acquisition time for recording the energy loss spectra was lower. For comparison purposes, the relative energy scales for this work are considered accurate to $0.2\,eV$ although the error on the absolute values might be larger due to systematic errors in the calibration procedure. The relative scales are accurate since a constant and reproducible value of the spectrum offset in the spectrometer is used throughout the measurements. The absolute values of the energy scale depend on the precise knowledge of the offset which can be obtained via calibrations with known standards based on edge energies from the literature. Our energy scales, however, are consistent with systematic EELS measurements on a series of titanates carried out by Brydson et al. [10] using a cold-field emission high-resolution EELS system.

3. Results and discussion

3.1. Crystal structure of $Nd_{2/3}TiO_3$ and $Nd_{0.70}TiO_3$

The crystal structure of $Nd_{2/3}TiO_3$ has not been reported before. It was anticipated that $Nd_{2/3}TiO_3$ would be isostructural with $La_{2/3}TiO_3$ which was described in Pban on a $\sqrt{2}a \times \sqrt{2}a \times 2a$ type perovskite cell, where it refers to the pseudo-cubic subcell, sometimes called the aristotype [11]. Quite recently, it has been argued that the true structure of $La_{2/3}TiO_3$ is better described in Cmmm with $2a \times 2a \times 2a$ cell [12]. While crystals of $Nd_{2/3}TiO_3$ exist, as described above, attempts to solve the structure from X-ray diffraction data collected on a "single" crystal were unsuccessful. This is probably due to micro domain twinning and this problem is under current investigation. While it has not yet been possible to prepare polycrystalline $Nd_{2/3}TiO_3$ in sufficient amounts to collect neutron or synchrotron X-ray powder data, the preparation of compositions quite close to $x = 0.33$ is relatively easy. Thus, powder neutron diffraction data were collected on a sample with $x = 0.30$, i.e. $Nd_{0.70}TiO_3$. While these are rather low-resolution data, the structure obtained from a Rietveld refinement should suffice for the purposes of this study. A more comprehensive investigation of the structures of phases in the $Nd_{1-x}TiO_3$ system with x near 0.33 is currently under way using high-resolution powder neutron and X-ray single crystal data. The neutron data set was refined both in *Pban* and *Cmmm*. The results for the *Cmmm* model were clearly better as shown by comparison of the standard Rietveld agreement indices, $R_{wp} = 5.96[7.52]$, $\chi^2 = 3.67[6.25]$ and $R_{Bragg} = 7.31[13.1]$, where those for the *Pban* model are in square brackets. The refined unit cell and atomic parameters for the *Cmmm* model are given in Table 1

Table 1
Refined unit cell and atomic parameters for $Nd_{0.70}TiO_3$

Space group: *Cmmm* (#65)
$a = 7.696(2)\,\text{Å}$
$b = 7.670(3)\,\text{Å}$
$c = 7.731(2)\,\text{Å}$

Atom	Site	x	y	z	B (Å^2)	Occ.
Nd(1)	4g	0.262(2)	0	0	0.51	0.98(2)
Nd(2)	4h	0.259(3)	0	1/2	0.52	0.42(2)
Ti	8n	0	0.240(2)	0.259(2)	0.28(14)	
O(1)	4i	0	0.276(2)	0	0.44(19)	
O(2)	4j	0	0.194(2)	1/2	0.54(24)	
O(3)	4k	0	0	0.200(2)	2.63(43)	
O(4)	4i	0	1/2	0.282(2)	0.71(22)	
O(5)	8m	1/4	1/4	0.233(1)	2.19(20)	

R_{wp} (%) = 5.96
$\chi^2 = 3.67$
R_{Bragg} (%) = 7.31

Note: As the displacement factors (B) and the site occupation factors are strongly correlated, the B were fixed at reasonable values and the occupation factors were refined for the Nd sites.

Table 2
Selected interatomic distance and angles for $Nd_{0.70}TiO_3$

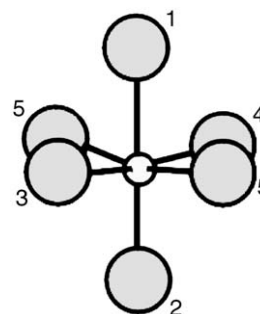| Ti–O distances (Å)		O–Ti–O angles (deg)		Ti–O–Ti angles (deg)	
Ti–O1	2.02(1)	O3–Ti–O4	171.2(2)	Ti–O5–Ti	168.1(3)
Ti–O2	1.90(1)	O5–Ti–O5	167.2(2)	Ti–O4–Ti	169.8(4)
Ti–O3	1.90(2)	O1–Ti–O2	177.4(5)	Ti–O2–Ti	159.0(5)
Ti–O4	2.00(1)	O2–Ti–O3	93.4(5)		
Ti–O5 × 2	1.936(2)	O5–Ti–O2	96.3(2)		
		O4–Ti–O2	95.4(3)		

Fig. 1. The geometry of TiO_6 octahedron in $Nd_{0.70}TiO_3$.

and selected inter-atomic distances and angles in Table 2. The Nd site occupation factors indicate that the vacancies are ordered, primarily in the 4h site at $z = \frac{1}{2}$. Note from Table 2 and Fig. 1 that the TiO_6 octahedron is highly distorted from the ideal geometry. This distortion may be reflected in some of the EELS spectra. The average Ti–O distance is 1.95 Å, in good agreement with the sum of the Shannon radii, 1.96 Å [13].

3.2. ELNES. Ti L_{23}-edge and O K-edge spectra for $Nd_{2/3}TiO_3$ and other various $3d^0$ perovskites

It is of interest to compare the ELNES spectra of $Nd_{2/3}TiO_3$ with those for oxides with perovskite-related structures such as $CaTiO_3$, $SrTiO_3$ and $BaTiO_3$. All these perovskites have empty titanium $3d$ bands and are band insulators. The crystal structure of $Nd_{2/3}TiO_3$ has just been described. $BaTiO_3$ crystallizes in a tetragonal structure (space group $P4mm$) with an axial ratio $c/a = 1.016$, i.e., it is almost cubic [14]. As the temperature is lowered, titanium moves off-center in its octahedron to give a ferroelectric phase. $SrTiO_3$ has an undistorted cubic symmetry $Pm3m$ at room temperature, with unit cell parameter $a = 3.905$ [15]. $CaTiO_3$ crystallizes in an orthorhombic structure ($Pnma$) with $c/a = 1.421$ [16]. For all these materials, the Ti^{4+} is in octahedral coordination with oxygen, with all octahedra sharing corners.

Fig. 2 shows the titanium L_{23} absorption spectra of $Nd_{2/3}TiO_3$, $BaTiO_3$ and $SrTiO_3$ and $CaTiO_3$. The intensity of the spectra has been scaled with respect to peak A, for the purpose of comparison. The relative peak positions are summarized in Table 3. The four peaks in the spectra have been fitted using a 'multi-peak' Lorentzian model. The peak-width values, shown in Table 4, are the results of these fits.

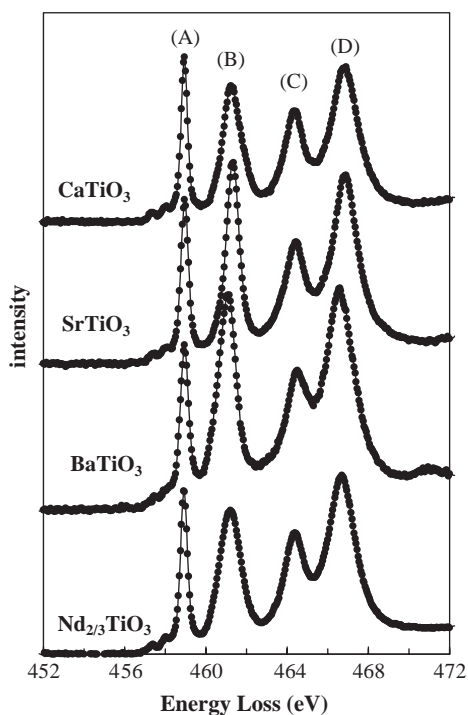As expected from the formal valency of Ti and the approximate octahedral coordination, $Nd_{2/3}TiO_3$,

Table 3
The relative peak energy loss values in the Ti L_{23}-edge spectra of different titanium oxides (eV)

	$CaTiO_3$	$SrTiO_3$	$BaTiO_3$	$Nd_{2/3}TiO_3$
A	458.939(3)	458.95(1)	458.95(1)	458.91(1)
B	461.29(1)	461.325(4)	461.055(4)	461.21(1)
C	464.38(1)	464.43(1)	464.50(1)	464.37(1)
D	466.82(1)	466.86(1)	466.59(1)	466.70(1)

Table 4
The peak width values in the Ti L_{23}- edge spectra of different titanium oxides

	$CaTiO_3$	$SrTiO_3$	$BaTiO_3$	$Nd_{2/3}TiO_3$
A	0.32(1)	0.40(1)	0.43(1)	0.35(1)
B	1.01(2)	0.74(1)	1.01(1)	1.13(3)
C	1.08(3)	1.26(3)	1.35(4)	1.09(4)
D	1.72(2)	1.70(2)	1.89(2)	1.92(3)

$BaTiO_3$, $SrTiO_3$ and $CaTiO_3$ have similar atomic multiplet spectra (Fig. 2). For these compounds, the electronic transitions occur from the titanium core $2p^63d^0$ level configuration to an excited $2p^53d^1$ state. The four samples show strong 'white lines' in the spin–orbit coupling of the $2p$ core hole levels of $2p_{3/2}$ (L_3) and $2p_{1/2}$ (L_2) absorption thresholds. The position of the L-edge signals depends on the oxidation state of the metal cation and, for the four Ti^{4+} compounds, the L_3 maximum is centered at about 458.9 eV. The average spin–orbit splittings for $CaTiO_3$, $SrTiO_3$, $BaTiO_3$ and $Nd_{2/3}TiO_3$ are on the order of 5.49(6), 5.545(3), 5.50(2), and 5.49(1) eV, respectively.

The fine structure of spin–orbit components in Fig. 2 is dominated by inter-atomic processes resulting in the 'crystal-field splitting' of titanium L-edges due to octahedrally coordinated Ti^{4+} ions. In the simplest interpretation, the lowest energy peak of each L-edge doublet is the transition to the t_{2g} states and the higher energy peak to the e_g states. The average splitting between the two main peaks in both the L_3 (ΔAB) and L_2 (ΔCD) edges for $CaTiO_3$, $SrTiO_3$, $BaTiO_3$ and $Nd_{2/3}TiO_3$ is 2.39(6), 2.40(4), 2.10(1), and 2.31(2) eV, respectively. It has been shown by detailed calculation that the energy splittings between the two main peaks in both the L_3 and L_2 doublets are in general not a direct measure of the actual crystal-field splitting [17]. Based on the same calculations however, we can estimate by inspection the crystal-field parameters from the measured splittings and the results for $CaTiO_3$, $SrTiO_3$, $BaTiO_3$ and $Nd_{2/3}TiO_3$ are 2.16, 2.17, 1.85 and 2.02 eV, respectively. For $SrTiO_3$, this crystal-field parameter estimated using this approach is larger than 1.8 eV reported by Abbate et al. [18] corresponding to the

Fig. 2. Titanium L_{23} ELNES of the perovskites $Nd_{2/3}TiO_3$, $BaTiO_3$, $SrTiO_3$, and $CaTiO_3$. The spectra have been shifted vertically for clarity.

ground state Ti^{4+} in octahedral symmetry but the values for the four materials constitute a self-consistent set and comparisons within the set should be valid. The average Ti–O bond distances for $BaTiO_3$, $SrTiO_3$, $CaTiO_3$, $Nd_{2/3}TiO_3$ are 2.005, 1.9552(4), 1.957(1), 1.95(1)Å, respectively [14–16]. By comparing the crystal field estimates and the bond lengths, we can see that the values of the crystal-field and the mean Ti–O bond lengths are similar for $CaTiO_3$, $SrTiO_3$ and $Nd_{2/3}TiO_3$ while that for $BaTiO_3$ is considerably longer. As the crystal-field is a reflection of the strength of the interaction between the metal and the ligand, we can directly see the correlation between the average Ti–O bond length and the crystal-field parameters. Based on the improved energy resolution of the monochromated system, which allows measurements where the width of spectral features is not significantly altered by the instrumental broadening as in conventional EELS measurements (with a resolution between 0.5 and 1 eV), we can tabulate the peak widths obtained from fitting to Lorentzians (Table 4). For both the L_3 and L_2 doublets, the e_g component is significantly broader than the t_{2g}. There are two major contributions to this effect, the first one being the strong core-hole contribution which sharpens the features at the near-edge threshold and the second arising from the much stronger interaction, and thus overlap of the e_g orbitals with the ligands in octahedra geometry. Among the most important broadening mechanisms are vibrational broadening due to mixing with excited vibrational states and dispersional broadening, due to metal/ligand interactions which leads to band broadening in the solid state. Note that while the t_{2g} line widths show only a small variation within this set of perovskites due to the strong core-hole effect sharpening the edge threshold, the e_g bandwidths show a considerable range. $SrTiO_3$ has the most narrow L_3 e_g resonance while those for $CaTiO_3$ and $BaTiO_3$ are 36% larger and that for $Nd_{2/3}TiO_3$ increases by more than 50%. These systematic trends can be roughly correlated with the Ti site symmetry in the crystal which is fully octahedral in $SrTiO_3$ [m-3m] but significantly lower in $CaTiO_3$ [-1], $BaTiO_3$ [4mm] and $Nd_{2/3}TiO_3$ [m]. Especially, for the latter two materials the absence of an inversion center permits mixing of Ti 4p and 3d orbitals. Similar site symmetry arguments have been advanced to explain extra e_g broadening in the L_3-edge spectra of $FeTiO_3$ and TiO_2 [17]. In our high-resolution spectra, it is also possible to observe much stronger multiplet structure below the t_{2g} peak for $SrTiO_3$, $CaTiO_3$, and $Nd_{2/3}TiO_3$ than for $BaTiO_3$.

The oxygen 1s absorption spectra for the same set of perovskite materials (Fig. 3) involves transitions from the oxygen 1s core level to unoccupied final states of p character centered on the oxygen atom due to selection rules. This absorption channel reflects therefore the O 2p bands that hybridize with the metal 3d and higher
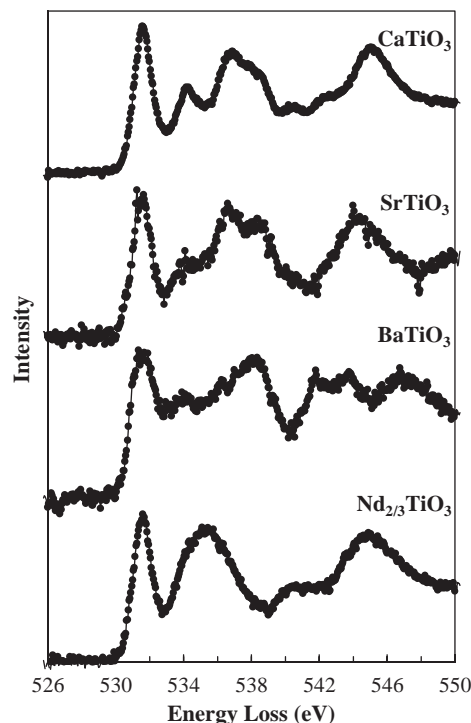

Fig. 3. Oxygen K-edge spectra for selected d^0 perovskites. The spectra have been shifted vertically for clarity.

energy orbitals. Due to this mixing, the O K-edge spectra also reflect the hybridization with the Ti empty states. For the purpose of comparison, the spectra have been scaled with respect to the strong peak just above the edge onset. The ELNES data obtained here for $SrTiO_3$ and $BaTiO_3$ are essentially the same as those reported by others from either XAS or EELS studies [20]. A characteristic feature of all of the spectra in Fig. 3 is the presence of a leading, relatively narrow peak in the energy range extending $\sim$3 eV above the edge onset. This reflects the unoccupied O 2p states hybridized with the narrow Ti t_{2g} states via 2p–3d interactions. The energy loss fine structure of the O K-edge, however, differs significantly from the structure seen in binary Ti oxides TiO and TiO_2 [19] where a well-resolved O 2p–Ti 3d (e_g) sub-band peak at $\sim$2 eV above the t_{2g} related peak is observed. While a weak peak occurs at the e_g band position for $CaTiO_3$, $SrTiO_3$ and $BaTiO_3$ at about 534 eV, the spectrum is considerably more complex than for the binary oxides. These extra features and the difference in the well-resolved t_{2g} and e_g components have been attributed to ligand interactions at higher energy with metal ns and np states from the group II atoms and to the strongly distorted octahedra in the binary oxides making the t_{2g} and e_g bands of comparable width and intensity [17]. For $Nd_{2/3}TiO_3$, the e_g peak is completely obscured suggesting even stronger mixing of the ligand and available Nd states. This is understandable in terms of the much less basic nature of Nd

relative to the group II elements and the availability of a range of low lying Nd states such as 5d, 6s and 6p.

3.3. ELNES spectra of $Nd_{1-x}TiO_3$ samples

The titanium L_{23} absorption spectra of $Nd_{1-x}TiO_3$ for vacancy compositions $x = 0$, 0.05, 0.12, 0.21, and 0.33 show systematic trends within the series (Fig. 4). The appearance of the $x = 0.33$ [$Nd_{2/3}TiO_3$] spectrum has just been explained as arising from the transitions between the $2p^63d^0$ ground state and the $2p^53d^1$ excited state taking into account the effect of the spin–orbit coupling and the crystal field. The $x = 0.0$ ($NdTiO_3$) spectrum is dramatically different and corresponds to 100% Ti^{3+} [19]. Here the transitions occur from a ground state with $2p^63d^1$ configuration to a $2p^53d^2$ excited state and indicate that as the Nd composition changes and the concentration of vacancies increases, the average valency of Ti is modified. Based on calculations of the $L_{2,3}$ spectra for all d^n configurations for a range of cubic crystal fields [O_h or m-3m] [17], we can compare our experimental data for $NdTiO_3$ with calculated spectra for Ti^{3+} and estimate, by inspection, an approximate cubic crystal field of $\sim$1.5 eV. Besides the systematic shift by $\sim$2 eV to higher energies, due to uncertainty in energy calibration procedure discussed in the experimental section, our results can be directly compared, in terms of energy resolution with the calculated spectra and the already published Ti 2p

$La_{1-x}Sr_xTiO_3$ XAS results for $x = 0-1$ obtained with a synchrotron [18].

The evolution of the EELS near edge structure of the solid solution $Nd_{1-x}TiO_3$ in Fig. 4 show essentially the same features as the XAS study of $La_{1-x}Sr_xTiO_3$ [18]. The spectra for $LaTiO_3$ and $NdTiO_3$ [$x = 0$] are clearly identical, apart from the presence of $\sim$10% TiO_2 impurity in the former XAS measurements, and the derived crystal field is 1.5 eV for both. This is not surprising as these are isostructural materials [8]. The differences between $SrTiO_3$ [$x = 1$ in $La_{1-x}Sr_xTiO_3$] and $Nd_{2/3}TiO_3$ [$x = 0.33$] were discussed in the preceding section. Intermediate compositions in both solid solution series represent mixed valence Ti^{3+}/Ti^{4+} situations and thus a control of the Ti oxidation state with the change in composition. To facilitate comparisons of the spectra, Table 5 lists the Ti^{4+} fraction in the two systems. The direct comparison of the spectra with the relevant compositions yielding a comparable Ti^{4+} fraction show nearly indistinguishable features indicating that the Ti bonding is not affected by the La or Nd ions.

For $x = 0$ compound in $Nd_{1-x}TiO_3$ solid solution, the average Ti–O–Ti bond angle is $150°$ and this increases to $\sim$166° with 1/3 substitution of Nd^{3+}-sites with vacancies in $x = 0.33$. The increase in bond angle, which is the result of the replacement of the larger Ti^{3+} by the smaller Ti^{4+}, requires a reduction of Ti–O bond length. As a result, $3d$ t_{2g} sub-band is broadened by the increase of inter-atomic overlap. The Ti L_{23} spectra of
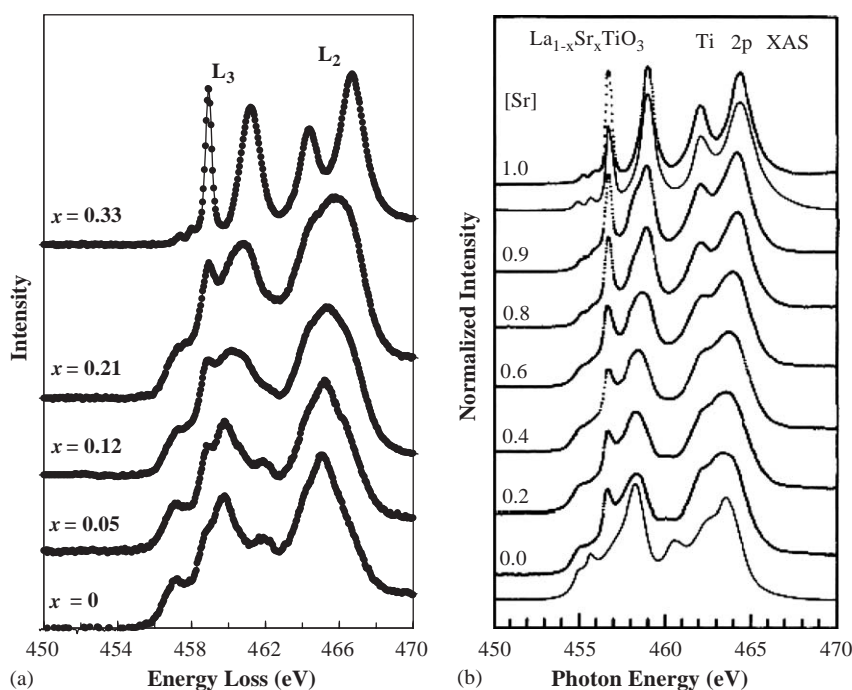

Fig. 4. (a) Ti L_{23} absorption spectra of $Nd_{1-x}TiO_3$ as a function of vacancy compositions (x). The spectra have been shifted vertically for clarity. (b) Ti 2 p XAS spectra of $La_{1-x}Sr_xTiO_3$ as a function of Sr x content. Taken from Ref. [18].

$Nd_{1-x}TiO_3$ for $x = 0.05$, 0.12 and 0.21 are not proportional superpositions of the parent $x = 0$ and 0.33 spectra. This is to be expected as the crystal field splitting values increase systematically with the increase of the average Ti valence from $x = 0$ to 0.33.

The oxygen 1s absorption near-edge spectra of $Nd_{1-x}TiO_3$ for x between 0 and 0.33 (Fig. 5) also show systematic trends in the features. The intensities have been scaled to match at the central peak B. Our measurements show that the position of peak A moves ~ 1.0 eV to higher energy as x decreases from 0.33 to 0. The theoretical amount of Ti^{3+} in the formulae of the mixed valent compounds, along with the relative energy loss values are summarized in Table 6. As mentioned earlier, the observation of O K-edge spectra in transition metal oxides directly contains information on the covalent interactions between the O 2p and transition metal 3d states both in the occupied and unoccupied states. Covalency has a direct effect on the shape and energy levels of the filled states with O 2p character and

therefore has direct consequences on the empty O 2p levels due to hybridization with the 3d transition metal orbitals. Thus, the intensity of the transitions is affected by the degree of admixing between the p-states with the 3d-states and is dependent on the local symmetry and oxidation state of the transition metal ion. Again, these results should be compared directly to the published spectra for $La_xSr_{1-x}TiO_3$ [21]. Strong similarities are apparent.

In the solid solution $Nd_{1-x}TiO_3$, the intensity ratio between peak A and B, $I(A)/I(B)$, increases strongly as the Ti^{4+} concentration is increased from $x = 0$ to 0.33 as also shown in the reported $La_xSr_{1-x}TiO_3$ system [21]. The growth of intensity in peak A, from the $x = 0$ to 0.33 compositions (Fig. 5), is indicative of a significant increase in the mixing of O 2pπ states with the

Table 5
Comparison of the nominal Ti^{4+} content in the $Nd_{1-x}TiO_3$ and $La_{1-x}Sr_xTiO_3$ (or $La_xSr_{1-x}TiO_3$) solid solutions

x in $Nd_{1-x}TiO_3$	%Ti^{4+}	x in $La_{1-x}Sr_xTiO_3$	%Ti^{4+}	x in $La_xSr_{1-x}TiO_3$	%Ti^{4+}
0.0	0	0.0	0	1.0	0
0.05	15	0.20	20	0.8	20
0.12	36	0.40	40	0.6	40
0.21	63	0.60	60	0.4	60
0.33	100	1.0	100	0.0	100

Table 6
The relative peak energy loss values in the O K-edge spectra as a function of vacancies (x) in $Nd_{1-x}TiO_3$

x	Calculated Ti^{3+} amount (%)	Peak energy values[a] (eV)		
		A	B	D
0	100	532.6	536.5	545.1
0.05	85	532.2	536.0	545.1
0.12	64	531.8	535.6	545.1
0.21	37	531.7	535.5	545.1
0.33	0	531.7	535.4	545.1

[a]The absolute values are uncertain due to possible zero-loss peak shifts although the relative energy scale in the series is accurate to about 0.2 eV. Within each spectrum the energy scale is accurate to better than 0.05 eV.
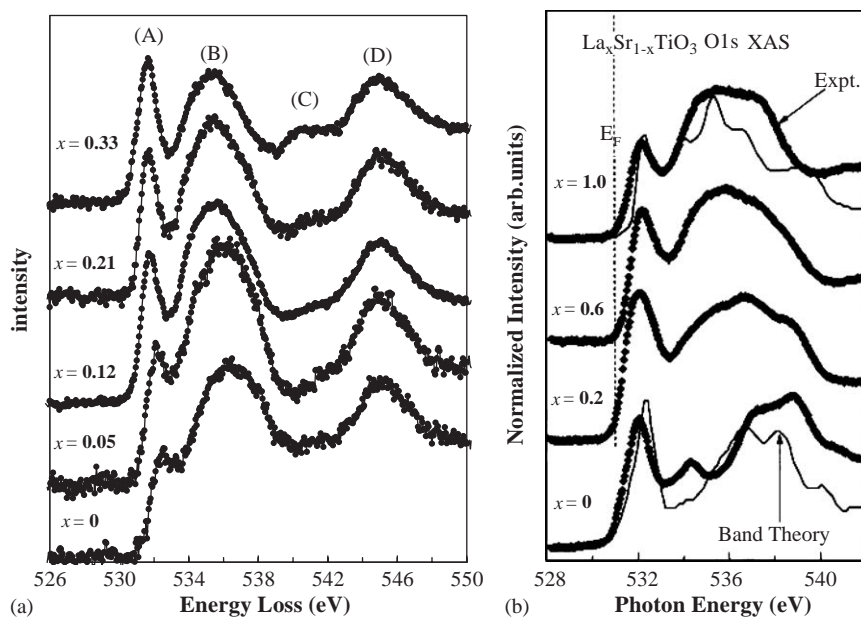

Fig. 5. (a) EELS spectra of the O K-edge from $Nd_{1-x}TiO_3$ as a function of vacancy compositions (x). The spectra have been shifted the vertically for clarity and normalized in intensity with respect to peak labeled B. (b) Oxygen 1s XAS spectra of $La_xSr_{1-x}TiO_3$ as a function of x. Taken from Ref. [21].
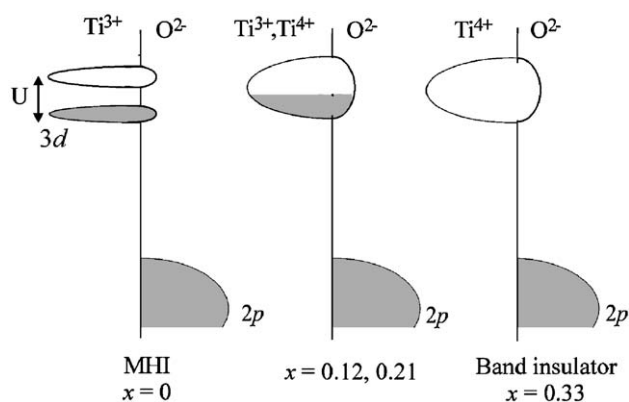
Fig. 6. The DOS picture of a Mott–Hubbard insulator (MHI) and charge transfer insulator (CTI). The compositions $x = 0.12$ and 0.21 are metallic.

unoccupied titanium $3d$ states which in turn are being depleted as the Ti valency evolves from Ti^{3+} to Ti^{4+}. The increase in the intensity of this peak due to the O $2p$–Ti $3d$ hybridization reflects the concomitant increase of unoccupied states due to the change in Ti valency from $3+$ to $4+$ as illustrated in Fig. 6.

In the Mott–Hubbard $NdTiO_3$ compound, the transitions observed in the O K-edge probe the higher lying states at the oxygen site (shown in Fig. 6) arising from the O $2p$–Ti $3d$ hybridization. The lowest lying Ti $3d$ band is split by an energy "U" into an upper Hubbard band and a LHB due to the coulomb repulsion of the $3d$ electrons. The value of U for $LaTiO_3$ has been measured recently as $\sim 4\,eV$ from combined photoemission and inverse photoemission data [22]. A similar value is expected for $NdTiO_3$. With the introduction of vacancies on Nd, holes appear in the Ti $3d$ band and, as suggested in our experimental data of the Ti L_{23} edge, the fraction of Ti^{4+} systematically increases. As these materials are not purely ionic, this effect is reflected not only in the Ti levels but also in the O $2p$ levels as evidenced by the O K-edge data. As the Ti $3d$ band is emptied, (see the Ti site in Fig. 6), the oxygen near edge structure shows that there is a concomitant increase in the O $2p$–Ti $3d$ hybrid empty states. The intensity increase in the lowest energy peak in the O K-edge at $532\,eV$ with increased vacancy concentration is direct evidence of this effect and correlates with the increased fraction of Ti^{4+}. Furthermore, such significant changes cannot be simply explained by changes in the symmetry around the oxygen atoms or the vacancies. The growth of this feature is difficult to discern at low vacancy concentration, $x = 0.05$ (15% Ti^{4+}) but becomes clearly marked at $x = 0.12$ (36% Ti^{4+}) where the Ti^{3+} feature at $533\,eV$ appears only as a shoulder to the high energy side. At the other extreme, when the system is a band insulator with the $x = 0.33$ composition, the lower Ti $3d$ band is entirely empty and the O $2p$ states reflect the increased density of unoccupied states (Fig. 6).

4. Summary and conclusions

The vacancy doped mixed valence titanate system $Nd_{1-x}TiO_3$, $x = 0.0$ to 0.33, has been studied using high-resolution EELS spectroscopy both at the Ti $L_{2,3}$-edge and the O K-edge. As the crystal structure of the $x = 0.33$ member, $Nd_{2/3}TiO_3$, had not been reported, its structure was refined from neutron powder diffraction data in $Cmmm$. The TiO_6 coordination geometry was found to be strongly distorted from octahedral symmetry (m-$3m$) to point symmetry (m). Comparison of the Ti $L_{2,3}$-edge spectra of $Nd_{2/3}TiO_3$ with the related perovskites $CaTiO_3$, $SrTiO_3$ and $BaTiO_3$ with the enhanced energy resolution show systematic differences which can be partially rationalized in terms of parameters such as the average $\langle Ti–O \rangle$ distance and the Ti-site symmetry. As well, the less basic nature of Nd in comparison to the Group II elements, Ca, Sr and Ba, and the availability of low lying $5d$, $6s$ and $6p$ levels results in transitions which obscure the O $2p$–Ti $3d$ e_g unoccupied hybrid feature in the O K-edge spectra of $Nd_{2/3}TiO_3$.

In the corresponding spectra for the mixed valence $Nd_{1-x}TiO_3$ series, there are strong similarities with published results for the related $La_{1-x}Sr_xTiO_3$ system, especially the Ti $L_{2,3}$-edge data that indicates that the valency of Ti is controlled by the Nd composition. This supports the Mott–Hubbard model for these materials, i.e., that the lowest lying transitions are to Ti d-states. The corresponding marked changes in the O K-edge data show that there is a significant hybridization between the O $2p$ and Ti $3d$ states.

References

[1] J.H. Rask, B.A. Miner, P.R. Buseck, Ultramicroscopy 21 (1987) 321.
[2] H. Kurata, C. Colliex, Phys. Rev. B 48 (1993) 2102.
[3] F.M.F. deGroot, J. Electron Spectrosc. Rel. Phenom. 67 (1994) 529.
[4] S. Lazar, G.A. Botton, F.T. Tichelaar, M.-Y. Wu, H.W. Zandbergen, Ultramicroscopy 96 (2003) 535.
[5] G. Amow, N.P. Raju, J.E. Greedan, J. Solid State Chem. 155 (2000) 177–188.
[6] Y. Tokura, Y. Taguchi, Y. Okada, Y. Fujishima, T. Arima, K. Kumagai, Y. Iye, Phys. Rev. Lett. 70 (14) (1993) 2126.

[7] M.J. MacEachern, H. Dabkowska, J.D. Garrett, G. Amow, W. Gong, G. Liu, J.E. Greedan, Chem. Mater. 6 (1994) 2092.

[8] D.A. MacLean, H.K. Ng, J.E. Greedan, J. Solid State Chem. 30 (1979) 35.

[9] J.N. Reimers, J.E. Greedan, M. Sato, J. Solid State Chem. 72 (1988) 390.

[10] R. Brydson, H. Sauer, W. Engel, in: M.M. Disko, C.C. Ahn, B. Fultz (Eds.), Transmission Electron Energy Loss Spectrometry in Materials Science, The Mineral, Metals and Materials Society, 1992.

[11] A.M. Glazer, Acta Crystallogr.: Struct. Crystallogr. Cryst. Chem. B 28 (11) (1972) 3384.

[12] C.J. Howard, Z. Zhang, J. Phys.: Condens. Matter 15 (6) (2003) 4543.

[13] R.D. Shannon, Acta.Crystallogr. A 32 (1976) 751.

[14] J. Harada, T. Pedersen, Z. Barnea, Acta Crystallogr. A 26 (1970) 336.

[15] Y.A. Abramov, V.G. Tsirelson, V.E. Zavodnik, S.A. Ivanov, I.D. Brown, Acta Crystallogr. B 51 (1995) 942.

[16] R.G. Buttner, E.N. Maslen, Acta Crystallogr. B 48 (1992) 644.

[17] F.M.F. de Groot, J.C. Fuggle, B.T. Thole, G.A. Sawatzky, Phys. Rev. B 41 (1990) 928.

[18] M. Abbate, F.M.F. de Groot, J.C. Fuggle, A. Fujimori, Y. Tokura, Y. Fujishima, O. Strebel, M. Domke, G. Kaindl, J. van Elp, B.T. Thole, G.A. Sawatzky, M. Sacchi, N. Tsuda, Phys. Rev. B. 44 (11) (1991) 5419.

[19] C. Mitterbauer, G. Kothleitner, F. Hofer, P.C. Tiemeijer, B. Freitag, H.W. Zandbergen, Microsc. Microanal. 9 (Suppl. 3) (2003) 086.

[20] R. Brydson, H. Sauer, W. Engel, F. Hofer, J. Phys.: Condens. Matter 4 (1992) 3429.

[21] A. Fujimori, I. Hase, M. Nakamura, H. Namatame, Y. Fujishima, Y. Tokura, M. Abbate, F.M.F. de Groot, M.T. Czyzyk, J.C. Fuggle, O. Strebel, F. Lopez, M. Domke, G. Kaindl, Phys. Rev. B. 46 (1992) 9841.

[22] T. Higuchi, D. Baba, T. Takeuchi, T. Tsukamoto, Y. Taguchi, Y. Tokura, A. Chainani, S. Shin, Phys. Rev. B 68 (2003) 104420.